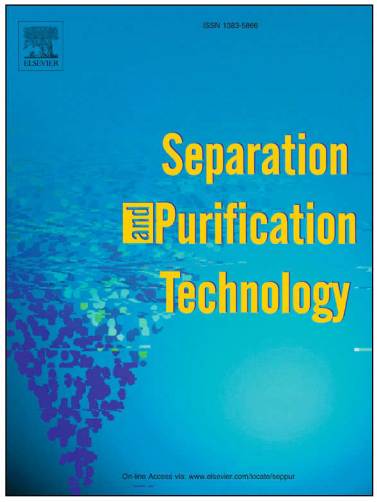

Lanthanum tungstate membranes for H_2 extraction and CO_2 utilization: fabrication strategies based on sequential tape casting and plasma-spray physical vapor deposition

M.E. Ivanova, W. Deibert, D. Marcano, S. Escolástico, G. Mauer, W.A. Meulenberg, M. Bram, J.M. Serra, R. Vaßen, O. Guillon

PII: S1383-5866(18)32978-2
DOI: https://doi.org/10.1016/j.seppur.2019.03.015
Reference: SEPPUR 15382

To appear in: *Separation and Purification Technology*

Received Date: 28 August 2018
Revised Date: 11 January 2019
Accepted Date: 5 March 2019

Please cite this article as: M.E. Ivanova, W. Deibert, D. Marcano, S. Escolástico, G. Mauer, W.A. Meulenberg, M. Bram, J.M. Serra, R. Vaßen, O. Guillon, Lanthanum tungstate membranes for H_2 extraction and CO_2 utilization: fabrication strategies based on sequential tape casting and plasma-spray physical vapor deposition, *Separation and Purification Technology* (2019), doi: https://doi.org/10.1016/j.seppur.2019.03.015

Lanthanum tungstate membranes for H_2 extraction and CO_2 utilization: fabrication strategies based on sequential tape casting and plasma-spray physical vapor deposition

M.E. Ivanova[a]*, W. Deibert[a], D. Marcano[a], S. Escolástico[c], G. Mauer[a], W.A. Meulenberg[a,d], M. Bram[a], J.M. Serra[c], R. Vaßen[a], O. Guillon[a,b]

[a] *Forschungszentrum Jülich GmbH, Institute of Energy and Climate Research IEK-1: Material Synthesis and Processing, 52425-Jülich, Germany*

[b] *Jülich Aachen Research Alliance: JARA-Energy, Forschungszentrum Jülich GmbH, D-52425 Jülich, Germany*

[c] *Instituto de Tecnología Química (Universitat Politècnica de València-Consejo Superior de Investigaciones Cientifícas), Av. Los Naranjos s/n, E-46022 Valencia, Spain*

[d] *University of Twente, Faculty of Science and Technology, Inorganic Membranes, P.O. Box 217, 7500 AE Enschede, The Netherlands*

*** Corresponding Author**

Dr. Mariya E. Ivanova

Forschungszentrum Jülich GmbH

Institute of Energy and Climate Research IEK-1: Materials Synthesis and Processing

52425-Jülich, Germany

Phone: 0049-(0)-2461-615194

Fax: 0049-(0)-2461-612455

E-mail: m.ivanova@fz-juelich.de

Abstract

In the context of energy conversion efficiency and decreasing greenhouse gas emissions from power generation and energy-intensive industries, membrane technologies for H_2 extraction and CO_2 capture and utilization become pronouncedly important. Mixed protonic-electronic conducting ceramic membranes are hence attractive for the pre-combustion integrated gasification combined cycle, specifically in the water gas shift and H_2 separation process, and also for designing catalytic membrane reactors. This work presents the fabrication, microstructure and functional properties of Lanthanum tungstates ($La_{28-x}W_{4+x}O_{54+\delta}$, LaWO) asymmetric membranes supported on porous ceramic and porous metallic substrates fabricated by means of the sequential tape casting route and plasma spray-physical vapor deposition (PS-PVD). Pure LaWO and W site substituted LaWO were employed as membrane materials due to the promising combination of properties: appreciable mixed protonic-electronic conductivity at intermediate temperatures and reducing atmospheres, good sinterability and noticeable chemical stability under harsh operating conditions. As substrate materials porous LaWO (non-substituted), MgO and Crofer22APU stainless steel were used to support various LaWO membrane layers. The effect of fabrication parameters and material combinations on the assemblies' microstructure, LaWO phase formation and gas tightness of the functional layers was explored along with the related fabrication challenges for shaping LaWO layers with sufficient quality for further practical application. The two different fabrication strategies used in the present work allow for preparing all-ceramic and ceramic-metallic assemblies with LaWO membrane layers with thicknesses between 25 and 60 µm and H_2 flux of ca. 0.4 ml/min.cm^2 measured at 825 °C in 50 vol.% H_2 in He dry feed and humid Ar sweep configuration. Such a performance is an exceptional achievement for the LaWO based H_2 separation membranes and it is well comparable with the H_2 flux reported for other newly developed dual phase cer-cer and cer-met membranes.

Keywords: *Solid State Proton Conductors, Ceramic Mixed Protonic-Electronic Conductors, Lanthanum Tungstate Membranes, Metal Supported Ceramic Membranes, Crofer22APU, H_2 Separation, CO_2 Utilization, Membrane Reactors, Tape Casting,* plasma spray-physical vapor deposition *PS-PVD*

1. Introduction

Hydrogen (H_2) permeable dense ceramic membranes are a key element for the efficient operation of electrochemical conversion devices, as well as H_2 separators and membrane reactors. In the context of energy conversion and storage systems, H_2 related membrane technologies for intermediate- and high-temperature (400-900 °C) applications emerge as a hot topic. Membrane processes can be efficiently integrated into advanced system concepts for i) H_2 generation as fuel used in mobile and stationary applications (steam electrolysers, water gas shift (WGS) reactors, H_2 extractors); ii) efficient and clean conversion of chemical to electrical energy (fuel cells, H_2 gas turbines); iii) utilization of H_2 and CO_2 in chemistry and petro-chemistry (catalytic membrane reactors) [1-11]. In fact, H_2 extraction from gas mixtures or its consumption in a chemical reaction by means of catalytic membrane reactor can intensify the process and significantly increase per-pass product yield while reducing the efficiency loss and final product cost. One example as an illustration is the water gas shift reaction expressed with Eq. 1 according to which steam is added to oxidize carbon monoxide to carbon dioxide, while H_2 is generated.

$$CO + H_2O \longrightarrow CO_2 + H_2 \qquad (\Delta H^0 = -41.09 kJ/mol) \qquad \text{(Eq. 1)}$$

Being slightly exothermic, the WGS reaction is limited by the thermodynamic equilibrium at high temperatures, while high temperatures are required to ensure the necessary reaction rates. Maximal carbon monoxide conversion is observed at 200-250 °C, however the reaction is kinetically limited therefore takes place very slowly. At temperatures 500-550 °C the rate increases but only limited conversion is achieved due to the exothermal nature of the WGS reaction. To overcome these limitations, simultaneous carrying out of the WGS reaction and CO_2/H_2 separation can be realized by means of a H_2 selective membrane in a catalytic membrane reactor. Literature data show that CO_2 separation is substantially associated with efficiency losses. Franz has studied the energetic and economic aspects of CO_2 separation in the pre-combustion power plant concept [12] and reported that an Integrated Gasification Combined Cycle (IGCC) with CO_2-separation via physical Selexol washing leads to 10.3% efficiency losses compared to an IGCC without CO_2-separation. A catalytic membrane reactor, using a H_2 selective membrane, significantly decreases the efficiency losses compared to conventional techniques such as physical or chemical absorption [13]. The resulting efficiency increase is realized by combining the two process steps - WGS reaction and gas separation- into a single more efficient step. The continuous removal of hydrogen in that case shifts the

reaction equilibrium to the product side, hence, WGS reaction can proceed at temperatures above the conventionally applied ones (500-550 °C).

For the successful membrane operation in the above mentioned application, membrane materials need to retain their phase and chemical composition at elevated temperatures in atmospheres containing H_2, H_2O, CO, CO_2, and impurities such as CH_4, SO_x, H_2S, HCl, KCl, NaCl, KOH, NaOH, originating from the coal or biomass gasification. Such extreme operating environments and elevated temperatures of operation are critical for the majority of H_2 selective material classes (polymers, microporous SiO_2, Carbon-SiO_2 molecular sieves or Pd-based alloys, as well as some ceramics), leading to material decomposition, membrane disintegration and performance degradation. In this context, scientific community faces the challenge of identifying, developing and exploring stable and well performing ceramic membrane materials for a variety of chemical reactions including WGS reaction, as well as suitable membrane-catalyst systems, which remain active and stable under relevant operating conditions [14-17].

Various ceramic candidates based on cerates and zirconates for high temperature H_2 separation have been studied over the past two decades. Numerous substituents on Ce site (M) in $BaCe_{1-x}M_xO_{3-\delta}$ and $SrCe_{1-x}M_xO_{3-\delta}$ have been examined to reveal their effect on H_2 permeation properties of these materials. Barium Cerates $BaCe_{1-x}M_xO_{3-\delta}$ with M = Y and Ru [18], Nd [19] and Srontium Cerates $SrCe_{1-x}M_xO_{3-\delta}$ with M = Y [20-22]; Sm [23]; Eu [23]; Tb [24]; Tm [25,26]; Zr and Tm [27-29]; Zr and Yb [29]; Zr and Eu [30]; Yb [31] have been extensively studied due to their very promising performance, while only a few zirconate based compounds $BaZr_{1-x}(Y,Mn)_xO_{3-\delta}$ [32], $SrZr_{1-x}Y_xO_{3-\delta}$ [33] have attracted the attention due to their lower performance. Furthermore, several dual phase materials (ceramic-ceramic or ceramic-metallic composites) appeal as very promising candidates for H_2 separation membranes. Unprecedented H_2 flux of 0.61 ml/min.cm^2 for a 500 µm thick $BaCe_{0.8}Eu_{0.2}O_{3-\delta}$-$Ce_{0.8}Y_{0.2}O_{2-\delta}$ ceramic-ceramic composite membrane was achieved at 700 °C [34]. Such performance at 700 °C is only comparable with the flux measured in the temperature range from 750 °C to 900 °C for a few other ceramic-ceramic composite membranes [35-38], as well as for a few ceramic-metallic composite membranes with significant amounts of Ni or precious metal Pd [39,40]. Despite the very promising H_2 permeation properties reported for the widely studied cerates and based on them dual phase composite membranes, their application under the aforementioned gas environments (H_2, H_2O, CO, CO_2, CH_4, SO_x, H_2S, HCl, KCl, NaCl, KOH, NaOH) at elevated temperatures remains limited due to their insufficient thermo-chemical stability. Zirconates and based on them composite materials or $BaZr_{1-x}Ce_xO_{3-\delta}$ solid solutions with high Zr contents

exhibit far better chemical stability compared to the cerates. Nevertheless these materials have insufficient interface performance- e.g. blocking grain boundaries with depleted proton content which affects the protonic and ambipolar conductivity and leads to significantly lower levels of H_2 permeation.

On the contrary, Lanthanum tungstates (LaWO) based compounds offer a good compromise between performance and stability, therefore in the present study pure and W site substituted LaWO were chosen as excellent membrane candidates.

Lanthanum tungstates are defective fluorite structured compounds with general formula $La_{28-x}W_{4+x}O_{54+\delta}$ where x=0.74-1.08 (La:W=5.75-5.3) and δ=1.11-1.62 (in the literature also known as $La_{6-x}WO_{12-\delta}$) and attract attention as proton conductors since 2001 [41-47]. The sulfur and carbon tolerance has been proven for Lanthanum tungstate LaWO [48,49], BZYM [32], and several $BaZr_{1-x}Ce_xO_{3-\delta}$ based compositions and cells [50-53]. Superior chemical stability against numerous contaminants (HCl, KCl, NaCl, KOH, NaOH) was evidenced for the LaWO compared to $BaZr_{1-x}Ce_xO_{3-\delta}$, therefore they are especially attractive for the aforementioned applications [49].

It is well known that LaWO is a mixed protonic-electronic conductor under humid reducing atmospheres at temperatures between 600 and 900 °C, while it exhibits predominant proton conductivity until 600 °C [41-43]. Protons are incorporated into the crystal lattice of LaWO (Eq. 2) according to the hydration reaction given below in Kröger-Vink notation (Eq. 3) [54].

$$yH_2O_{(v)} + La_{28-x}W_{4+x}O_{54+\delta}v_{2-\delta} \leftrightarrow La_{28-x}W_{4+x}O_{54+\delta+y}H_{2y}v_{2-\delta-y} \quad (\delta = 3x/2) \qquad \text{(Eq. 2)}$$

$$H_2O_{(g)} + v_O^{\bullet\bullet} + O_O^X \rightarrow 2OH_O^{\bullet} \qquad \text{(Eq. 3)}$$

Protons diffuse through the lattice and so give rise to proton conductivity, which for LaWO is in the range of 10^{-3} S/cm at 800 °C [43]. This value is the highest one for the proton conductivity amongst the number of reported Lanthanide tungstates and it correlates to the higher crystal symmetry in the case of La tungstates [42,43]. Therefore, fabrication of a membrane consisting predominantly of single cubic LaWO phase is essential for the membrane performance. As postulated by the general formula, La to W ratio in the range of 5.3-5.75 is crucial for the single phase formation [44,46]. Beyond this single phase domain, the undesired secondary phases La_2O_3 and $La_6W_2O_{15}$ are segregated and in larger amount they might compromise the mechanical stability of the membrane [55]. It has been, however, reported that this domain shifts to higher La contents when W site is Mo or Re substituted [56,57]. In general, W site substituents of mixed valence as Mo and Re boost the electronic conductivity of LaWO, which is

negligible at temperatures up to 800 °C. Mo and Re substituents have resulted in the most effective amongst a number of other tested cations [46,58,59]. In a case of sufficiently fast surface reaction (ensured by the high T and/or a suitable catalyst), the ambipolar conductivity $\sigma_{H^+} t_{e^-}$ (where t_{e^-} is the transport number of electrons) of Mo and Re substituted LWO was significantly improved [46], resulting in a higher H_2-flux j_{H_2} compared to the non-substituted compound (7- to 10-fold increase respectively measured on bulk Mo-LaWO and Re-LaWO samples at 700 °C [59]). Further studies on the crystal structure and hydration properties of these substituted compounds (for substitution concentration of up to 20 mol.%) can be find in [56,57] where the effect of substituents was thoroughly enlightened.

In fact, apart from the previously mentioned fundamental studies, there is a significant lack of application oriented research on dense ceramic membranes for H_2 separation in general, and specifically on LaWO membranes. Most of the aforementioned performance studies have been carried out on bulk ceramic samples based on variety of cerates, zirconates and LaWO. Only a very few of them elucidate the H_2 permeation resulting from supported membranes with thickness in the µm range [2 µm in [31]; 20 µm in [38]; 25 µm in [60,61]; 50 µm in [22]; 150 µm in [25] and offer a fundamental understanding of the underlying transport processes. The major reason for this in our understanding relates with the fabrication challenges to shape flat reproducible structures consisting of a defect free functional membrane layer deposited onto a thick porous supporting layer. Fabrication of such structures is a highly complex process, especially because a number of materials properties (e.g. physical properties of the starting powders, thermal expansion of substrate and membrane, etc.) needs to be tailored, as well as the processing and sintering parameters to be suited for a specific manufacturing route.

In this paper, two industrially viable fabrication techniques, sequential tape casting (STC) and plasma spray-physical vapor deposition (PS-PVD), were applied for the manufacturing of supported LaWO membranes. As the H_2 flux is inversely dependent on the membrane thickness, membrane layers of several ten µm supported onto chemically and thermally compatible thicker porous layers were aimed in the present work. We furthermore explore and verify the formation of high quality LaWO functional layer on porous ceramic (LaWO and MgO) and metallic (Crofer22APU stainless steel) supporting layers, as well as we establish the sets of suitable fabrication parameters at lab scale which are furthermore applicable for the development of industrially relevant membrane sizes (as future prospective). Substrate materials in this work were selected based on their thermal and chemical compatibility with the LaWO membrane material to shape high quality all-ceramic (ceramic membrane/ceramic

substrate) and ceramic-metallic (ceramic membrane/metallic substrate) assemblies. The formation of substituted LaWO membranes supported on LaWO and MgO substrates via the tape casting approach is being considered as well. In this paper we offer an insight into the fabrication aspects of LaWO cubic phase, its formation and gas tightness by means of the two afore mentioned processing techniques, along with membrane performance estimation.

2. Experimental part

The tape casting technology was employed for the preparation of i) full ceramic assemblies (ceramic membranes supported on porous ceramic substrates) consisting of a LaWO membranes supported on LaWO and MgO substrates and ii) Crofer22APU supports used furthermore for the PS-PVD made ceramic-metallic assemblies (ceramic membranes supported on porous metallic substrate). LaWO membranes supported on porous Crofer22APU were fabricated by means of PS-PVD. Table 1 summarizes the fabricated assemblies, the processing technique used and the applied thermal treatment.

Table 1. Summary of the samples fabricated via the sequential tape casting (STC) and plasma spray-physical vapor deposition (PS-PVD).

Sample name	Membrane	Support	Method	Thermal treatment
$LaWO_{mem}/LaWO_{sub}$	LaWO	LaWO	STC	1450°C/3h, Air
$LaWO_{mem}/MgO_{sub}$	LaWO	MgO	STC	1450°C/3h, Air
$Mo\text{-}LaWO_{mem}/LaWO_{sub}$	Mo-LaWO	LaWO	STC	1450°C/3h, Air
$Mo\text{-}LaWO_{mem}/MgO_{sub}$	Mo-LaWO	MgO	STC	1450°C/3h, Air
$Re\text{-}LaWO_{mem}/LaWO_{sub}$	Re-LaWO	LaWO	STC	1450°C/3h, Air
$Re\text{-}LaWO_{mem}/MgO_{sub}$	Re-LaWO	MgO	STC	1450°C/3h, Air
$LaWO_{mem}/Crofer_{sub}$	LaWO	Crofer22APU	PS-PVD	No
$Crofer_{sub}$	No	Crofer22APU	STC	1100°C/2h, Ar

2.1. Membrane fabrication by tape casting

Tape casting has been proven a successful technique suitable also for further scale up for manufacturing of planar ceramic components [62,63] including SOFCs [64] and gas separation membranes [65], including LaWO membranes [66-68]. In particular the "sequential tape casting" (STC) developed at IEK-1 allows preparing the porous but mechanically robust supporting

(SOFC anode) layer and the much thinner dense (electrolyte) layer (typically 5-30 µm thick, preferably 5-15 µm) in a single process. Casting first the functional membrane layer over a polymeric foil and afterwards applying the substrate layer allows for manufacturing of supported defect free membranes with high surface quality, which would be otherwise hard to achieve. Tape casting furthermore enables the combination of different materials in green state, both ceramic and metallic. In any case one limitation is the required sintering step typically under oxidizing which is an essential drawback for the fabrication of ceramic-metallic assemblies.

2.1.1. Starting ceramic powders

The physical properties of all ceramic powders used in the tape casting processing are summarized in Table 2.

LaWO powder synthesized via the solid state reaction (LaWO-SSR)

The LaWO powder used for the membrane preparation was synthesised via the solid state reaction (SSR). For this purpose, stoichiometric amounts of La_2O_3 (99.999%, Sigma Aldrich) and WO_3 (99.995%, Sigma Aldrich) were milled in ethanol. After drying, the powder mixture was heated at 1500 °C for 12 h to accomplish the solid state reaction. The resulting powder was additionally milled in a planetary ball mill and sieved (32 µm mesh size). The mean particle size d_{50} of 0.8 µm and the specific surface area of 1.9 m²/g were estimated by means of laser diffraction and BET analysis.

LaWO powders synthesized via the modified Pechini method (LaWO-P)

Due to its higher stoichiometric precision Pechini method was used to synthesize 20 mol.% Re and 20 mol.% Mo substituted LaWO. As precursors, $LaN_3O_9{\cdot}6H_2O$ (lanthanum nitrate, Merck), $H_{42}N_{10}O_{42}W_{12}{\cdot}H_2O$ (ammonium tungstate, Sigma Aldrich), $HReO_4$ (Re acid, Alfa Aesar), $H_{24}Mo_7N_6O_{24}$ (ammonium molybdate, Sigma Aldrich) were used in addition to $C_6H_8O_7{\cdot}H_2O$ (citric acid, Merck) and $C_2H_6O_2$ (ethylenglycol, Merck). Synthesis procedure is described elsewhere [46,69]. For the complete removal of the organic components, powders were heat treated at 900 ºC/3h. To adapt the properties of resulting powder to the tape casting process, additional pre-calcination and milling steps were carried out. The resulting powders (1200 ºC/3h + milling) were furthermore employed for the membrane fabrication. As it can be seen from the table, the mean particle size d_{50} of 1.0 µm and the specific surface area of 1.77 m²/g level well with the values obtained for the LaWO powder produced via the SSR.

Commercial LaWO powder (LaWO-C)

For the substrate preparation commercially available LaWO powder with La/W ratio of 5.4 (CerPoTech, Norway) was used. The powder was produced by spray pyrolysis and calcined at 600 °C [70] resulting in initial specific surface area of 7 m²/g, therefore it was not directly suitable for the tape casting processing. An additional thermal treatment and milling steps were necessary for further tailoring the powder properties to the fabrication method.

Commercial MgO powder (MgO-C)

MgO powder with d_{50}=7.7 µm and specific surface area of 6.6 m²/g was commercially supplied (Sigma Aldrich). As in the case of LaWO-P and LaWO-C for fabricating porous substrates powder properties were adapted to the tape casting by annealing and milling before being used. MgO was selected as a substrate material as alternative to the LaWO due to its chemical and thermal compatibility with LaWO [68,71] but also due to its lower price considering future membrane size scale up.

Table 2. Physical properties of the ceramic powders used in the tape casting processing. SSR-Solid State Reaction, P-Pechini, C-Commercial, HT+ additional heat treatment.

Powder	Temperature (°C)	Time (h)	Milling/ Sieving	D_{50} (µm)	Particle size distribution	Specific surface area A_{spec} (m²/g)
LaWO-SSR	1500	12	Y/Y	0.8	Monomodal	1.9
LaWO-P	900	3	As synthesized	13.6	Bimodal	9.76
LaWO-P- HT+	1150	3	N/N	1.7	Bimodal	2.72
LaWO-P- HT+	1150	3	Y/Y	0.8	Monomodal	2.69
LaWO-P- HT+	1200	3	N/N	16.2	Bimodal	1.44
LaWO-P- HT+	1200	3	Y/Y	1	Monomodal	1.77
LaWO-C	600	-	As delivered	0.9	Monomodal	7
LaWO-C- HT+	1200	3	N/N	2	Bimodal	0.3
MgO-C	-	-	As delivered	7.7	Monomodal	6.6
MgO-C- HT+	1200	3	Y/Y	2.5	Monomodal	5.2

2.1.2. Cer-cer assemblies by sequential tape casting

As mentioned briefly above, the sequential tape casting consists of casting first the membrane layer onto the PET (polyethylene terephthalate) foil (thickness 100 µm, Karo Electronics Vertriebs GmbH, Germany), which moves with controlled speed into the vented chamber of the tape cast device KAROcast300-7 by KMS Automation GmbH Germany. After the complete drying of the membrane layer, the substrate layer was cast on top so that mostly defect-free functional membrane layers can be produced. Details on the slurry preparation can be found elsewhere [68,69]. LaWO and MgO supports were cast using solvent-based slurry with rice starch (particle size 2-8 µm) as pore former in amounts of 25 wt.% and 15 wt.%, respectively. Blade gap of 1 mm resulted in substrate thickness of ca. 400 µm, while a gap of 100 µm resulted in 30 µm thick membrane layer, both in final sintered state (1450 °C, 3h), respectively. Before the sintering step, samples with diameter of 22 mm were punched out of the dried plastic tape so that after sintering and grinding specimen with diameter of 15 mm were obtained.

2.2. Membrane fabrication by PS-PVD

The PS-PVD process was used to deposit LaWO ceramic layers onto Crofer22APU stainless steel porous substrates thus forming ceramic-metallic assemblies. Such metal supported membranes enable integration by conventional techniques as welding in e.g. a metal designed membrane reactor [72]. No high temperature co-firing of the PS-PVD processed assemblies is required [73,74] as in the case of the tape cast asymmetric structures. However, annealing at 900 °C in Ar and air was carried out to prove the stability of the sprayed LaWO membranes under elevated operation temperatures. The as sprayed membranes can be used directly after the PS-PVD fabrication, since during the plasma spraying the crystal structure formation is completed. In any case, a number of process parameters (plasma gas composition, plasma temperature, torch power, spraying distance, additional O_2 supply in the chamber, etc.) has to be controlled in order to prepare membranes with the desired crystal structure, phase composition and gas tightness. Therefore, the PS-PVD fabrication of high quality LaWO membranes is a laborious not trivial process, especially considering the phase and structural complexity of the LaWO material and the novelty on this particular subject. To the best of our knowledge, this is the first work reporting on the PS-PVD fabrication of asymmetric LaWO membranes and their H_2 permeation performance.

2.2.1. LaWO powder feedstock

The feedstock material was provided by Oerlikon Metco, Wohlen, Switzerland. Particle size distribution was estimated by laser diffraction (d_{10}=7 µm, d_{50}=11 µm, and d_{90}=17 µm). Single cubic phase LaWO was ascertained by Rietveld refinement of X-ray diffraction (XRD) patterns.

Prior to spraying, the as-delivered powder with spherical morphology was dried at 80 °C for 24 h in air to avoid agglomeration and to favor its flowability.

2.2.2. Manufacturing of porous metallic supports

Crofer22APU stainless steel was selected as a support material for the LaWO functional membrane layers due to their well matching coefficients of thermal expansion: $CTE_{Crofer22APU}=12.3\cdot10^{-6}$ K^{-1} and $CTE_{LaWO}=11\text{-}12\cdot10^{-6}$ K^{-1}. No intermediate layers were applied. Substrates were manufactured by means of the tape casting on casting bank FGA500-SAMA, Germany. As starting powder, gas atomized ferritic steel Crofer22APU powder by H.C. Starck, Germany (powder fraction with a median of d_{50}=13.3 µm) was used. An alcohol-based slurry with solid load of 88 wt.% was produced, using ethanol as a solvent and a combination of binder (Mowital, Kuraray, Japan) and plasticizing agents. Slurry viscosity was 20 $\pm$ 2 Pa·s at shear rate of 1.8 s^{-1}. Green tape thickness after drying was in the range of 1150-1200 µm and samples with dimensions 70x70 mm^2 were cut out of this tape. Thermal treatment included three steps: de-binding at 600 °C for 30 min, pre-sintering at 900 °C in Ar and final sintering at 1100 °C for 2 h in Ar. The final thickness of the sintered samples was estimated to be 0.87-1.03 mm with an average porosity of ca. 30 vol.% (optically determined with SEM image analysis). To shape round samples with a diameter of 15 mm laser cutting was applied.

2.2.3. Cer-met assemblies by PS-PVD

The LaWO functional layers were deposited by means of the Multicoat PS-PVD system (Oerlikon Metco, Wohlen, Switzerland) with an O3CP torch. Our previous works on complex ceramic components [75-77] indicated sets of plasma spray parameters which have led to the formation of gas tight ceramic coatings with desired phase compositions and were taken into a consideration in the present work. The effect of various PS-PVD processing parameters (e.g. plasma composition Ar:He=100:30 slpm (T_{plasma}=7396 K) and 110:20 slpm (T_{plasma}=7790 K); 900 mm and 1000 mm spray distance, Crofer22APU stainless steel and graphite substrates, O_2 addition and different annealing procedures) on the LaWO membrane phase formation and microstructural characteristics has been considered in depth and it will be published soon [78]. Presently, we focus only on membranes manufactured under the following PS-PVD conditions: torch input power 90 kW (I=2000 A), $p_{chamber}$ 250 Pa (2.5 mbar), plasma composition Ar:He=110:20 slpm (slpm: standard liters per minute), T_{plasma} 7790 K, spray distance 900 mm, 4 slpm addition of O_2 in the chamber to account of the oxygen stoichiometry of the formed LaWO phase. The sample was mounted in a sample holder with a metallic mask, so that it was kept in position without being constrained during heating and cooling and the heat flow from the

samples was ensured. Coating times of 3 min were chosen resulting in layers with thickness of 40 to 60 µm. It should be mentioned here, that for the manufacturing of dense coatings the deposition of fast and perfectly molten splats instead of a gas phase deposition is used. After spraying, the samples were annealed at 900 °C for 3h in Ar and air to prove their stability at elevated temperatures.

3. Characterization techniques

3.1. Physical properties of the powders

The particle size distribution (PSD) and the specific surface area (BET) [79] of the starting powders for preparation of asymmetric structures were carefully monitored. For that Horiba LA-950 V2 by Retsch Technology and area-meter by Ströhlein with N_2 as measurement gas were used respectively.

3.2. Chemical and phase composition

The chemical composition of the samples was determined using Inductively Coupled Plasma-Optical Emission Spectrometry (ICP-OES). The error in this measurement was ± 3%. The oxygen content was determined by means of He carrier-gas hot-extraction including infrared (IR) absorption (LECO TCH-600, 0.5% relative standard deviation for O_2). Finally, the stoichiometry was calculated.

X-ray diffraction (XRD, D4 Endeavor - Bruker AXS with Cu-Kα radiation) was performed to determine the phases present in the LaWO coating “as-sprayed” and “as-annealed” in Ar or Air. Phase identification was carried out with ICDD PDF2-Database (Release 2004), ICSD Database (Release 2017) and X’Pert Highscore Plus (by PANalytical). The reference patterns correspond to the cards ICSD 252211 ($La_{6.75}W_{1.25}O_{13.5}$), PDF No. 01-074-2430 ($La_2O_3$) and ICSD 247427 ($La_6W_2O_{15}$) for phase identification. These references were then used as a starting model for the Rietveld analysis carried out with the TOPAS V 4.2 software.

3.3. Sintering properties

The tape cast LaWO and MgO single substrate layers were characterized with an optical dilatometer TOMMIplus by Fraunhofer ISC, Germany. A piece of green substrate tape was shaped to a cylindrical sample with known height h_0 which was then positioned within the instrument chamber and gradually heated up to 1500 °C with heating ramp of 1 °C/min and kept for 3 h at the maximal temperature. Images of the sample silhouette were periodically recorded (every 60s) during the heat treatment with a charge-coupled device (CCD) camera. For achieving high contrast, a monochromatic light source was mounted opposite to the camera.

Software TOMMI online (Fraunhofer ISC, Würzburg, Germany) was used to analyse the corresponding shrinkage of the samples.

3.4. Microstructure and topography

To investigate the microstructure and phase detection of the tape-cast samples, scanning electron microscopy (SEM) was performed with Ultra 55 Zeiss (Germany) equipped with EDX (INCA, Oxford Instruments, UK), acceleration voltage of 15 kV and a back-scattered detector. For fast microstructural screening, a Phenom electron microscope by FEI with a back-scattered electron detector and acceleration voltage of 5 kV was used. Porosity, layer thicknesses, and pore size of the samples in cross sections were quantified with the AnalySIS pro software (Olympus Soft Imaging Solutions GmbH). For the PS-PVD samples electron backscattering diffraction (EBSD) was used carried out with SEM JSM-7000F by JEOL equipped with "Hikari" camera for EBSD and an "Octane Plus-A" detector for EDX (both by Ametek-EDAX). At 20 KeV electron energy and using a probe current of approximately 30nA areas of 200 µm x 75 µm were measured with a step size of 100 nm. The data were collected with the software OIM Data Collection V 7.3 and analyzed with OIM Analysis V 8.0.

The shape and topography of the samples were monitored by means of non-contact surface measurement system CT350 T from Cyber Technologies using a confocal white light sensor. The *z*-resolution of the sensor was 0.1 µm and the spot size was 12 µm.

3.5. Helium (He) gas-tightness and H_2 permeation

In our fabrication efforts we aim at achieving a gas tight membrane (we specify this quality as post fabrication gas tightness). Such gas tightness mirrors the high quality of the fabricated membrane, and it is a sign of lacking micro- and macro-defects in the membrane layer (pinholes, connected open porosity, cracks). The presence of such defects in the membrane structure with thickness of several tens of µm will be deleterious for the membrane performance. Along with the SEM analysis to conclude on the microstructure and gas tightness of the assembled layers, He leakage testing is a quality control tool to confirm the defect free nature of the fabricated membrane as a whole before the H_2 permeation through the membrane is measured. In this sense, the post fabrication He leakage test is an intermediate control step to conclude about the membrane quality and suitability for the next characterization step. The He leakage rate through a sample with area of 1 cm^2 is defined to be 1 $hPa \cdot dm^3/cm^2 \cdot s$ (or 1 $mbar \cdot l/\cdot cm^{-2} \cdot s$) if in a vacuum-reservoir or respectively a pressure reservoir with a volume of 1 liter the pressure rises and respectively drops about 1 mbar in 1 second. He leakage test was

performed on sintered asymmetric membranes with Pfeiffer Vacuum ASM 340 leak detector. For this purpose, the membrane sample (area of 1cm²) was mounted into a holder with the membrane side facing the vacuum and pressure difference of 1000 hPa was applied. The permeating He was measured with a mass spectrometer and converted into the permeation rate per sample area expressed in [hPa·dm³/cm^2·s] or [mbar·l/s·cm^2]. The theoretical background of this measurement was reported elsewhere [80,81]. A value of $1 \cdot 10^{-4}$ hPa·dm³/cm^2·s was set as a post fabrication He leakage threshold. Membrane assemblies which exhibit He leak lower than the mentioned threshold can be furthermore used in the H_2 separation performance tests. The present work does not include a systematic study on how the manufacturing influences the gas tightness of the LaWO membrane. In any case this topic is of crucial importance and for that it has been already considered in significant details in our earlier study [68].

H_2 permeation tests were carried out in a double chamber quartz reactor, depicted schematically in Fig. 1. As shown in the figure, H_2 was separated from He (feed side: mixture of 50 ml/min H_2 and 50 ml/min He) by using Ar as a sweep gas (flow rate of 150 ml/min). The sweep side was humidified (p_{H2O} = 0.025 atm) and the feed side was kept dry.

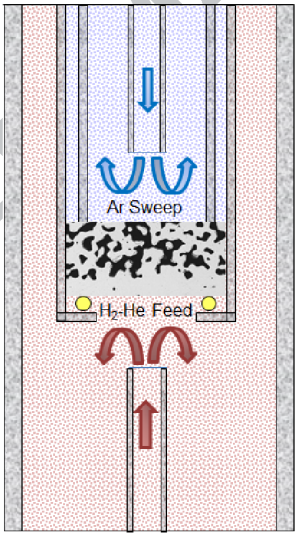

Figure 1. Schematic of the reactor chamber in which the membrane is gold-sealed and tested.

The asymmetric membrane assembly was sealed with the membrane side towards the feed stream, while the support was facing the sweep side. For sealing, gold rings were used at elevated temperature and the post sealing gas tightness was approved (He detection in the permeate side). The H_2 content in the permeate side was analysed using a micro-GC Varian

CP-4900 equipped with Molsieve5A and PoraPlot-Q glass capillary modules and He was continuously monitored to evaluate the leaks. All the membranes were catalytically activated. Pt catalytic layer was screen-printed on both sides of the LaWO bulk membrane. Pt was screen-printed on the dense membrane layer of the asymmetric structures whereas it was infiltrated in the porous substrates.

4. Results and discussion

After optimization of process parameters, asymmetric membrane samples consisting of $LaWO_{mem}/LaWO_{sub}$; $Mo\text{-}LaWO_{mem}/LaWO_{sub}$; $Re\text{-}LaWO_{mem}/LaWO_{sub}$; $LaWO_{mem}/MgO_{sub}$; $Mo\text{-}LaWO_{mem}/MgO_{sub}$ and $Re\text{-}LaWO_{mem}/MgO_{sub}$ were fabricated by tape casting. Multilayered tapes were cast defect free. Fig. 2 shows exemplary images of tapes in dry state before sintering. Selected tape cast samples in final sintered state (a,b) and a PS-PVD sprayed $LaWO_{mem}/Crofer_{sub}$ sample (c) are shown in Fig. 3.

Due to the different shrinkage rates of the membrane and substrate tape cast layers during the sintering as discussed elsewhere [68], fabrication of flat asymmetric membranes represents a major challenge, especially considering further scale up, therefore detailed knowledge about the sintering behavior of different layers and their careful matching was required. To ascertain the flat geometry with minimal deformations, a non-contact surface measurement system was also used. Fig. 3d depicts an exemplary image of a flat round shape $LaWO_{mem}/LaWO_{sub}$ after sintering. On the contrary, other types of tape cast assemblies fabricated in this study showed more serious deflection after sintering and this made their sealing in the H_2 permeation test rig very difficult. A number of samples could not withstand the mounting procedure and went broken.

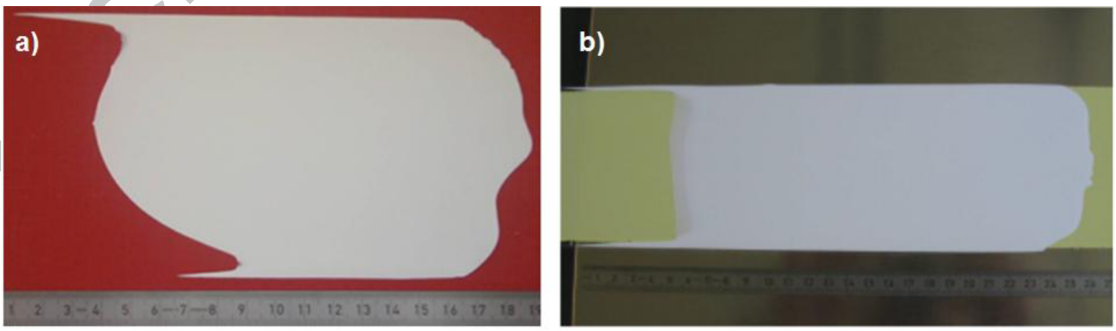

Figure 2. Images of tapes in dry state, a) $LaWO_{mem}/LaWO_{sub}$ (two tapes have white colour) and b) $Re\text{-}LaWO_{mem}$ (here seen as the yellowish-greenish coloured tape)/$LaWO_{sub}$ (white tape on top).

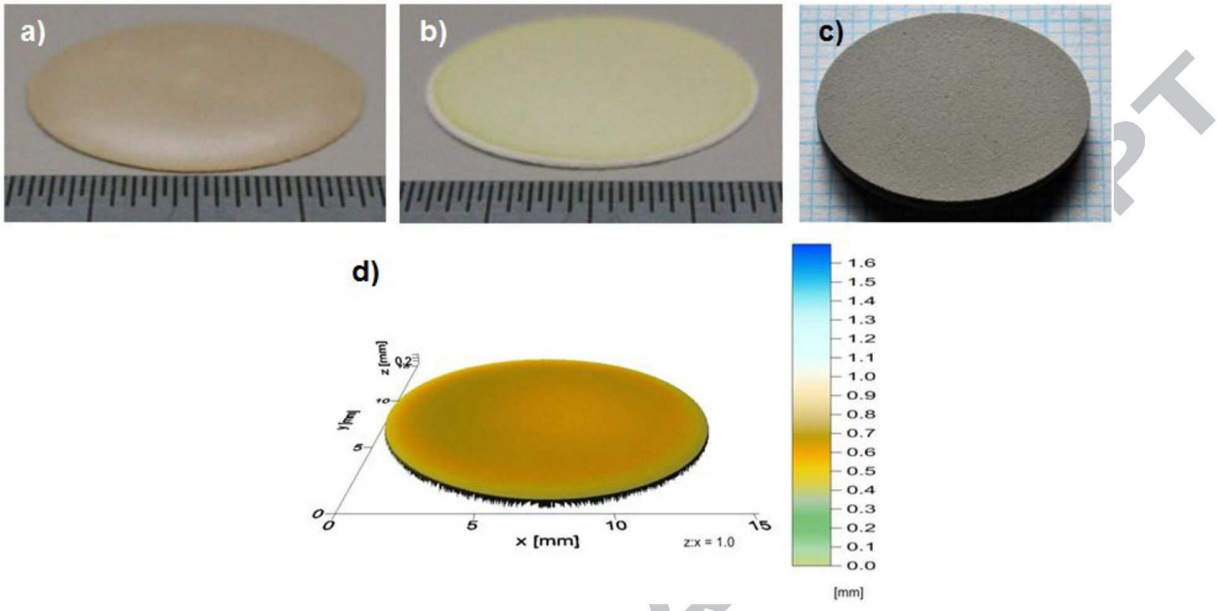

Figure 3. Images of asymmetric membranes: a) $LaWO_{mem}/LaWO_{sub}$ assembly by tape casting; b) $LaWO_{mem}/MgO_{sub}$ assembly by tape casting. Samples in a) and b) were sintered at 1450 °C for 6h; c) $LaWO_{mem}/Crofer_{sub}$ by PS-PVD; d) white light topographic image of $LaWO_{mem}/LaWO_{sub}$ (sintering at 1450 °C, 6h, with optimized slurry recipe, flat sample was obtained).

4.1. Structural and microstructural characteristics of the tape cast all ceramic assemblies

The formation of single cubic phase depends on the La/W ratio affected by the effective levels of substitution as well as on the thermal processing conditions. As already demonstrated in earlier works, La/W shifted from the single phase domain leads to formation of undesired secondary phases [44,46,55], both in substituted powder compounds (Fig. 4) and supported membrane assemblies (Fig. 5). Due to the enlarged crystal cell parameter caused by Mo substitution [82], a shift towards smaller diffraction angle can be observed, along with the secondary phase formation (peak splitting in Fig. 5 a, b). While the starting Mo-LaWO powders exhibited small amounts of La_2O_3, (Fig. 4 a, b), such segregations were not detected in the XRD pattern of the membrane. In the case of Re substitution, the XRD pattern of the membrane compared to that of the powder shows stronger inhomogeneity and higher presence of secondary phases. Therefore, further optimization of the phase composition and controlled

single phase formation will be required for both Mo-LaWO and Re-LaWO membranes shaped by means of tape casting before estimating their functional properties.

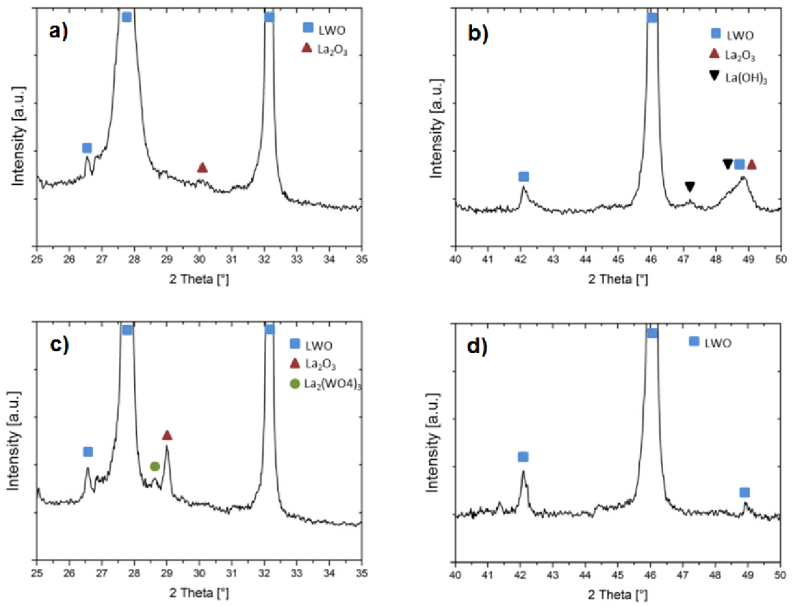

Figure 4. Excerpts of the XRD patterns of Pechini synthesized powders: a) and b) Mo-LaWO; c) and d) Re-LaWO.

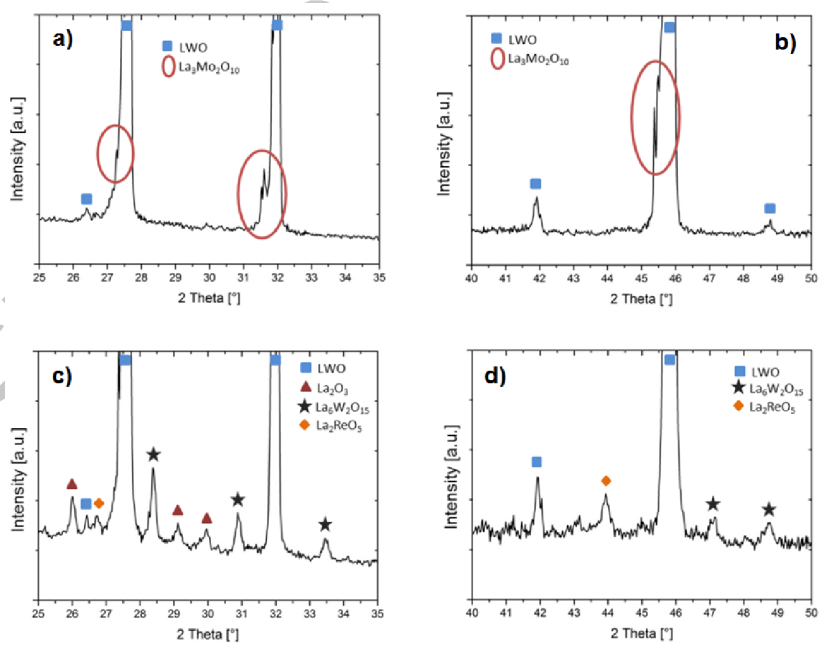

Figure 5. Excerpts of the XRD patterns of asymmetric assemblies via the tape casting: a) and b) Mo-$LaWO_{mem}/LaWO_{sub}$; c) and d) Re-$LaWO_{mem}/LaWO_{sub}$. Sintering carried out at 1450 °C for 6h for all samples.

The microstructure of sintered assemblies manufactured via the tape casting is depicted in Fig. 6, while the element diffusion pathways and estimated depths across the membrane-substrate interface are schematically depicted in Fig. 7. Polished cross-sections of assemblies supported on LaWO and MgO can be seen in Fig. 6 a)-c) and Fig. 6 d)-f), respectively. As it can be observed from the figure, the thickness of the LaWO membranes shaped on both LaWO and MgO substrates was in the range of 25-30 μm. The final substrate thicknesses after sintering was determined to be about 300-400 μm (not evident from the SEM micrographs).

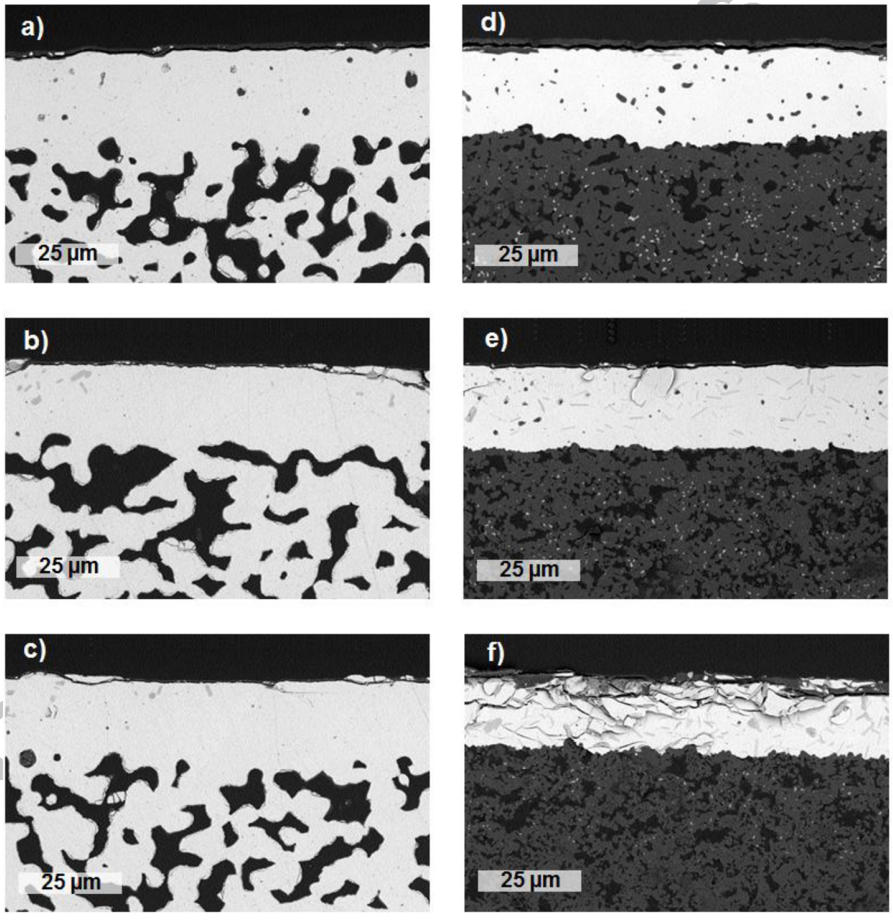

Figure 6. SEM images, polished cross-sections of assemblies manufactured via the tape casting: a) $LaWO_{mem}/LaWO_{sub}$; b) Mo-$LaWO_{mem}/LaWO_{sub}$ c) Re-$LaWO_{mem}/LaWO_{sub}$; d) $LaWO_{mem}/MgO_{sub}$; e) Mo-$LaWO_{mem}/MgO_{sub}$; f) Re-$LaWO_{mem}/MgO_{sub}$. Sintering was carried out at 1450 °C for 6h for all samples.

Secondary phases in several of the assemblies can be clearly observed from the SEM images in Fig. 6 as well as differently contrasting and shaped areas. The SEM-EDX analysis of the asymmetric Mo-LaWO and Re-LaWO membranes supported on LaWO (Fig. 6 b, c), discloses that the small dark areas were mostly composed of the $La_6W_2O_{15}$. Mo and Re diffusion towards the substrate could be ascertained which affected the initial membrane composition, i.e. La/W+Mo and La/W+Re ratios, resulting in small amounts of secondary phase segregations, as discussed previously. Despite that, the membranes exhibit sufficient integrity. For the LaWO supported assemblies the Mo and Re diffusion depth towards the substrate levels about 15-20 µm.

In the case of MgO supported structures, diffusion of Mg towards the LaWO membrane layer was observed in all three cases which can lead to partial substitution of La sites in LaWO and small decrease in proton conductivity [46]. However, La and W diffusion towards the MgO substrate takes also place with depth of about 60 µm for the pure LaWO and Mo-LaWO, leading to small secondary phase inclusions in the membranes (Fig. 6 d, e and Fig. 7 a, c). In the case of Re-$LaWO_{mem}$/MgO_{sub} assemblies La, W and Re diffusion depth levels ca. 20 µm versus the substrate (Fig. 7 d). The membrane showed significantly decreased integrity (Fig. 6 f), due to the formation of secondary phases. Interestingly, no diffusion of Mo towards the MgO substrate could be detected for Mo-$LaWO_{mem}$/MgO_{sub} (Supplementary Information, Fig. S1).

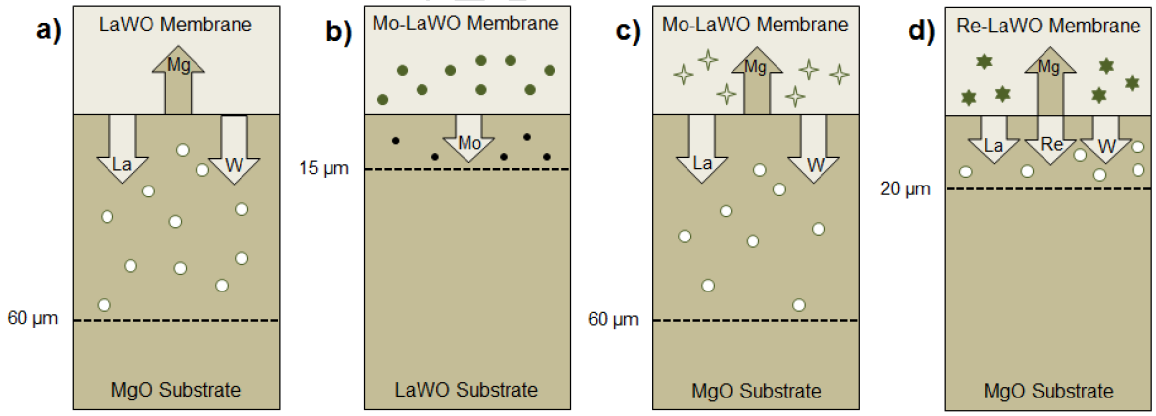

Figure 7. Schematics of cation diffusion pathways and depth (dashed line) in asymmetric assemblies as secondary phase formation driving force: a) $LaWO_{mem}$/MgO_{sub} [69]; b) Mo-$LaWO_{mem}$/$LaWO_{sub}$; c) Mo-$LaWO_{mem}$/MgO_{sub}; d) Re-$LaWO_{mem}$/MgO_{sub}; Different secondary phases are marked with symbols (○ La, W segregations; • $La_3Mo_2O_{10}$; ● $La_6W_2O_{15}$; ✧ and ✸ are multiple secondary phases, including La_2O_3, La_2ReO_5, $La_6W_2O_{15}$).

In addition to the microstructural characterization the gas tightness of sintered assemblies was monitored. Apart from the Re-$LaWO_{mem}/MgO_{sub}$ which showed mechanical disintegration due to multiphase membrane composition as observed in Fig.5 c, d and it was dismissed from further characterization, the rest of the samples were considered gas tight as ensured by the He leakage tests.

Apart from the tendency to form secondary phases due to the complex compositions and sensitive La/W ratios, another point of consideration is the major difference between the LaWO and MgO substrate microstructure (Fig. 6) originating mostly from the different amount of pore former used in the substrate slurry preparation (LaWO and MgO substrates with 25 wt.% and 15 wt.% pore former, respectively) and thus leading to significantly differentiating sintering properties of the MgO and LaWO substrate materials. Apparently, as evidenced by the shrinkage behavior of the two substrate materials determined by optical dilatometry in Fig. 8, the two substrate materials start shrinking at near the same temperature 1250 °C. The shrinkage of LaWO substrate is significantly accomplished at 1500 °C, while at the same temperature MgO has still not reached the plateau domain. These effects are well consistent with the SEM images of the MgO supported assemblies (Fig. 6 d, e, f) for which a large amount of very small pores within the single MgO particles can be observed. Connected pores forming channels can be also recognized in the images, but their size differs significantly from that in LaWO substrates, respectively less than 10 μm for MgO compared to more than 25 μm for LaWO at pore former amounts for LaWO and MgO, respectively of 25 wt.% and 15 wt.% and at the same sintering conditions. In the isothermal regime (3h at 1500 °C in Fig. 8) the two porous bodies shrinks continuously due to the residual substrate porosity, reaching total shrinkage of 36 % and 17 % for LaWO and MgO at the end of the temperature program, respectively.

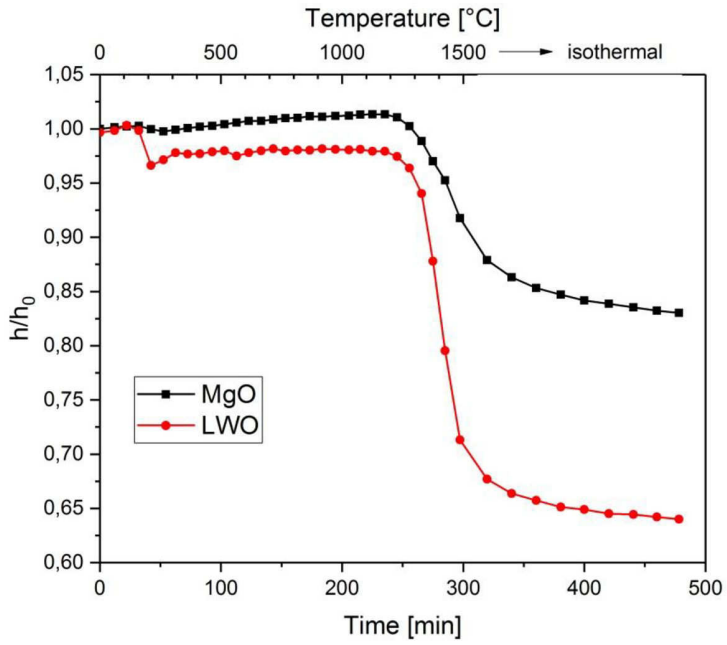

Figure 8. Shrinkage of the LaWO and MgO cylinders with initial height h_0 prepared from substrate single layers by tape casting. The change in relative sample height h/h_0 is depicted as function of the temperature and the time registered with TOMMIplus optical dilatometer.

Any possible impurities in the MgO raw material can contribute as well to the above discussed sintering effects of the MgO substrate. Chemical analysis of MgO ascertained 0.49 wt. % Ca and 0.12 wt.% Si along with Al, K, Na, P and Zr each in amounts less than 0.01 wt.%. It has been previously indicated that for impure MgO the impurities generally increase the value of the activation energy for grain boundary migration thus slowing the grain growth due to the increasing impurity accumulation at the grain boundaries as the grains grow larger and larger. Additionally the porosity appears to limit not only the grain size (small grain size formation can be evidenced for MgO substrate), but to decrease the grain growth rate as well [83].

Final substrate porosity of ca. 30 vol.% for LaWO substrate and less than 20 vol.% for MgO substrates was achieved. It is well known from the solid oxide fuel cells, which are multilayered structures consisting of solid oxide electrolyte membrane between two porous electrode layers, that porosity of 35-40 vol.% for the cell electrodes is required to ensure the optimal gas flow. Therefore sufficient porosity of the substrates in asymmetric membrane assemblies needs to be achieved to lower the polarization resistance at the membrane/substrate interface, as well as to establish a stable driving force across the complete asymmetric system. In this context, the

value of 20-30 vol.% for the supported assemblies might be not sufficient for the gas flow through the substrate. However, these were the first experiments to shape various supported assemblies and to observe their sintering and element interdiffusion effects. As next step in our research would be the deposition of interlayer between the membrane and specifically the MgO substrate to minimize the secondary phase formation, as well as employing larger amount of pore former for higher substrate porosity.

4.2. Structural and microstructural characteristics of the PS-PVD fabricated ceramic-metallic assemblies

LaWO dense membranes sprayed on Crofer porous substrate consist of the cubic phase with La/W ratio equal to 5.62, which is within the desired single phase domain. The analysis of as sprayed samples revealed presence of La_2O_3 secondary phase in a tolerable amount of ca. 2 %. The cross-section of a $LaWO_{mem}$/$Crofer_{sub}$ assembly can be seen from the SEM micrograph in Fig. 9, which reveals homogeneous and well adhering LaWO membrane layer with thickness of about 60 µm formed onto the rough steel surface. Furthermore, as Fig. 9 unveils, the LaWO membrane layer exhibits dense microstructure with less than 5% optically estimated porosity obtained without high temperature treatment in contrast to the required sintering temperatures of 1450-1500 °C for LaWO conventional densification.

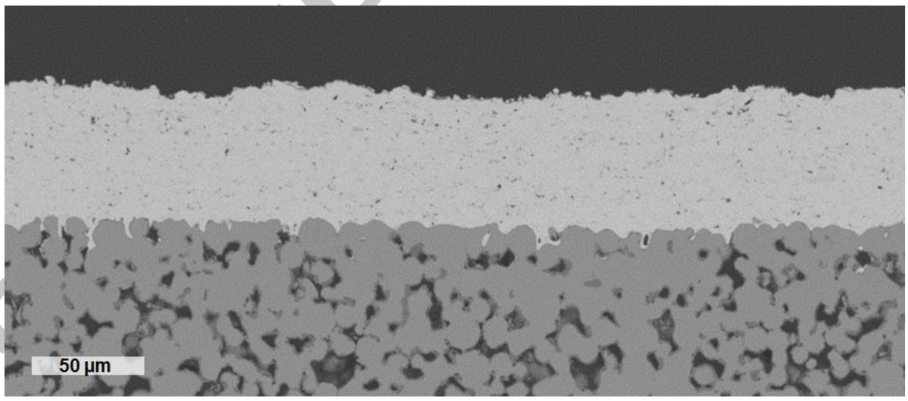

Figure 9. SEM image of $LaWO_{mem}$/$Crofer_{sub}$ assembly: cross section. Membrane thickness is around 60 µm.

To conclude on the membrane stability phase distribution after the annealing in Ar and air (both carried out at 900 °C for 3h EBSD analysis was carried out and the results are shown in Fir. 10. After annealing in Ar the secondary phase La_2O_3 remains negligible (Fig. 10 a), while the air annealing enhances the segregation of the two undesired phases La_2O_3 and $La_6W_2O_{15}$ (Fig. 10

b). Since the membrane is suited for operation in non-oxidative gas environments (p_{O2} lower than 10^{-5} atm) such segregations are not expected to become an issue for the stability.

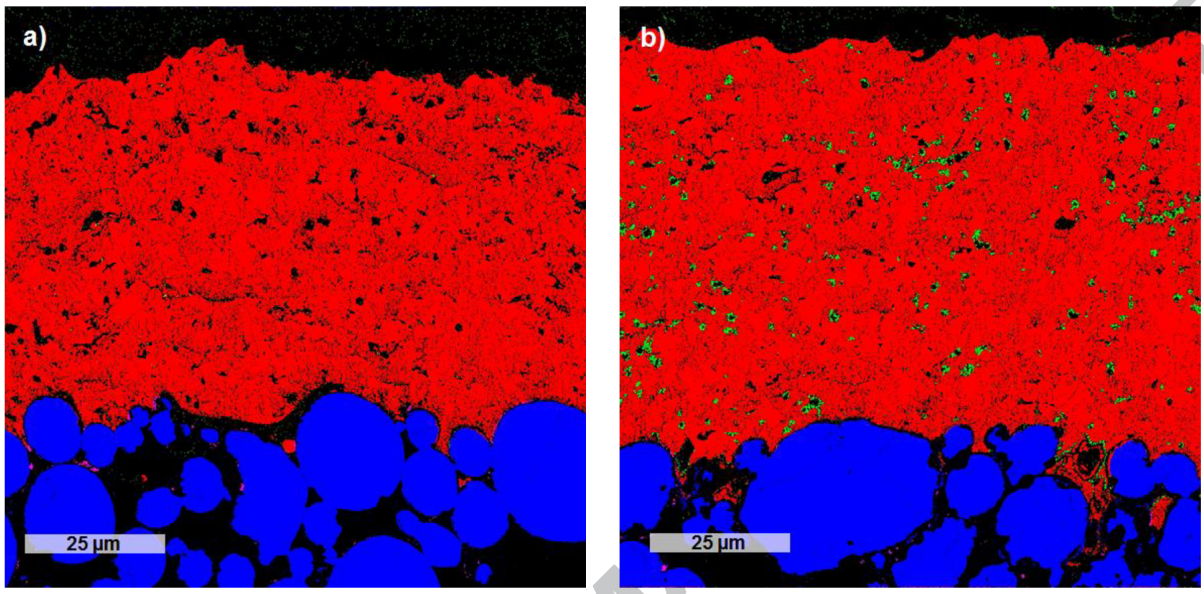

Figure 10. EBSD-image of cross sections of $LaWO_{mem}/Crofer_{sub}$ assembly: a) after annealing in Ar at 900 °C for 3h and b) after annealing in air at 900 °C for 3h for a sample prepared under addition of O_2 in the plasma chamber. LaWO phase in red, Crofer substrate in blue, secondary phase La_2O_3 in yellow is negligible in the two samples, while the segregations of $La_6W_2O_{15}$ in green are preferably formed in b).

4.3. H_2 permeation performance of $LaWO_{mem}/LaWO_{sub}$ $LaWO_{mem}/Crofer_{sub}$ assembies

H_2 permeation under elevated temperatures was tested for $LaWO_{mem}/LaWO_{sub}$ (sintered at 1450 °C for 6h in air) and $LaWO_{mem}/Crofer_{sub}$ (annealed in Ar). These two types of samples were suitable for functional measurements because they exhibited predominantly single phase composition of the membrane layer and sufficiently flat geometry to enable the sealing in the quartz glass reactor. It is worth mentioning that during the sealing of samples, several tape cast samples went broken due to the thin planar geometry (total sample thickness less than a half of mm), while several PS-PVD samples delaminated (membrane detached from the substrate). Regarding to the substrate porosity of the tape cast $LaWO_{mem}/LaWO_{sub}$ assembly, the value of about 30 vol.% might not be satisfactory for the optimal gas flow through the asymmetric structure (as earlier mentioned 35-40 vol.% porosity of the substrate would be required).

However, first tests of the membrane performance were carried out in application relevant conditions: temperature in the range 650-850 °C and in presence of water. In order to promote the surface reactions, Pt catalytic layers were screen-printed on both sides of the reference LaWO bulk sample. $LaWO_{mem}/Crofer_{sub}$ and $LaWO_{mem}/LaWO_{sub}$ membranes were also catalytically activated with Pt. For both dense membranes and porous supporting layers Pt was respectively screen-printed and infiltrated. Fig. 11 presents the hydrogen flux measured on reference bulk LaWO sample with thickness of 900 μm [59] and for the asymmetric membranes $LaWO_{mem}$/ $LaWO_{sub}$ and $LaWO_{mem}/Crofer_{sub}$ as function of the temperature. As it can be seen from the figure, the performance improves as the membrane thickness decreases (bulk versus the two asymmetric configurations) as the theory predicts (Eq. 4). On the other hand, the thicker $LaWO_{mem}/Crofer_{sub}$ (60 μm via the PS-PVD) shows better performance compared to the tape cast membrane with thickness of about 30 μm. Since these are the first result on this kind of LaWO asymmetric structures, future thorough consideration is required to confirm the observed effects and discuss on the underlying transport processes. Furthermore, the measured flux results both from H_2 permeation through the membrane and water splitting effect taking place at the sweep side of the membrane structure. As humidity is supplied at the sweep side of the membrane, it promotes oxygen diffusion across the membrane (Eq. 5) and thus giving rise to water splitting reaction. Further experiments are however needed in this direction in order to quantify these two processes underlying the overall registered H_2 flux.

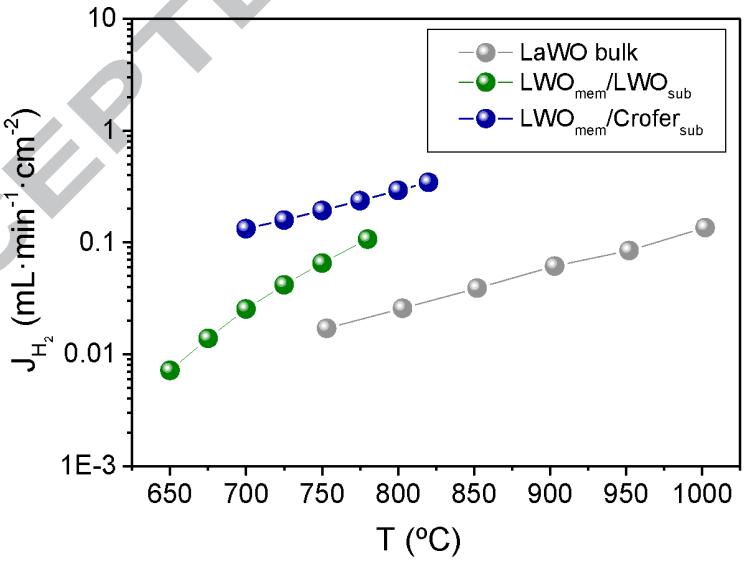

Figure 11. H_2 permeation as function of the temperature for LaWO (reference bulk sample), $LaWO_{mem}/LaWO_{sub}$ (tape casting) and $LaWO_{mem}/Crofer_{sub}$ (PS-PVD).

$$j_{H_2} = \frac{-RT}{2F^2L}\int_{I}^{II}\sigma_{H^+}t_{e^-}d\ln p_{H_2} \quad \text{(Eq. 4)}$$

$$j_{H_2} = \frac{-RT}{2F^2L}\int_{I}^{II}\sigma_{H^+}\left[t_{e^-}d\ln p_{H_2} + t_{O^{2-}}d\ln p_{H_2O}\right] \quad \text{(Eq. 5)}$$

The H_2 flux values in Fig. 11 are well comparable to the existing literature data. Summary of the H_2 performance data of asymmetric membranes is published in [38], while thickness normalized H_2 flux values are presented in [34]. At 825 °C the performance of the 60 µm thick PS-PVD LaWO membrane (ca. 0.4 ml/min·cm^2), as well as the extrapolated value at the same temperature for the 30 µm thick tape cast LaWO membrane (ca. 0.4 ml/min·cm^2) developed in this work levels considerably well with the value 0.68 ml/min·cm^2 measured on 20 µm asymmetric dual phase $BaCe_{0.65}Zr_{0.20}Y_{0.15}O_{3-\delta}$–$Gd_{0.2}Ce_{0.8}O_{2-\delta}$ membrane at 750 °C [38] and the same gas conditions as these used in the present work. Furthermore, H_2 flux of 0.14 ml/min·cm^2 was reported for a 25 µm thick tape cast LaWO membrane at 1000 °C [61], however the feed and sweep gas environments were different (feed wet 10% H_2 in Ar, sweep dry Ar) from these in the present work. It is worth mentioning, that the dual phase membranes consist of protonic- and electronic-conducting intercrossing phases and therefore their performance is usually far beyond that of a single phase compound. For that the dual phase membranes reveal higher performance at lower temperature and much larger thickness [34]. Nevertheless, there is not much available performance data reported on asymmetric membranes and especially on similarly fabricated and measured membranes, so that a reliable comparison can hardly be done. To the best of our knowledge the performance published in [61] is the only report on a tape cast asymmetric LaWO membrane, while no data is available for LaWO membrane fabricated by means of PS-PVD technique. Although the performance characteristics obtained for the LaWO membranes developed in the present work are quite promising, further optimization efforts as addressed below and performance prove are certainly required.

During the H_2 permeation measurements several issues arose which were detrimental for collection of more performance data: i) Fragility of the tape cast all ceramic assemblies during the sealing procedure. In this we use gold rings to connect and seal the specimen to the test chamber at elevated temperatures prior the H_2 permeation measurements. The tape cast assemblies were quite sensitive to the sealing due to their restricted thickness of 350-500 µm in

total. Furthermore, during the sintering some samples showed geometrical height deviations resulting in slightly deflected assemblies, which were then difficult to seal and measure properly. ii) Assembly delamination issues during the H_2 permeation tests in the case of the metal supported membranes fabricated by the PS-PVD technique. Additionally to these mechanical issues, the Pt activation of the assemblies has not been finally optimized, which will be one of our next experimental targets. We expect that the H_2 flux of our supported membranes will be furthermore significantly improved by optimizing the sealing, catalytic activation, as well as improving the mechanical stability of i) tape cast membranes by substrate lamination to increase the mechanical durability and ii) PS-PVD membranes by modifying the roughness of the substrate surface by appropriate technique to improve the adhesion of the ceramic membrane to the steel substrate.

Finally, as future prospective, due to the number of advantages offered by the tape casting and PS-PVD techniques, large scale membrane development is envisaged for subsequent integration in membrane modules and catalytic membrane reactors. In this way, proofs of different concepts for industrially relevant chemical processes can be offered based on proton conducting ceramic membranes.

5. Conclusions

The present work demonstrates the fabrication of gas-tight asymmetric membranes with thickness of 25-60 µm consisting of LaWO cubic phase (besides the substituted LaWO compositions) and supported on porous ceramic and porous metallic substrates. The employed fabrication methods- the tape casting and the PS-PVD, lead to the formation of defect free functional layers only after careful adjustment of the complex fabrication parameters and suitable material combination.

Predominantly single phase LaWO membranes was formed in the case of non-substituted material both on LaWO and Crofer22APU substrates and also for Mo substituted LaWO supported on porous LaWO. When MgO was used as a substrate enhanced interdiffusion effects could be observed leading to moderate to significant secondary phase segregations and in some case as e.g. Re substituted LaWO membrane to disintegration of the sintered structure. For that reason no performance estimation on multiphase membrane was performed. To minimize effectively the secondary phase formation in the substituted LaWO membranes caused by interdiffusion between the membrane and the substrate, barrier layers with graded microstructure need to be designed before estimating the performance of such substituted LaWO membranes. Furthermore, the phase composition of the PS-PVD fabricated LaWO

membrane revealed high phase purity. Even after annealing in Ar at 900 °C did not affect the phase composition, while the air annealing lead to more pronounced segregation of undesired secondary phases compared to the phase composition of the membrane as sprayed.

The substrates microstructure revealed porosity in the range of <20 to 30 vol.%, respectively, for the MgO substrates and for both the LaWO and Crofer22APU substrates. The lower pore former amount used for the MgO substrate slurry preparation, as well as the purity of the starting MgO powder determined the quite significant difference in the sintering behavior and the microstructure compared to the LaWO and the metallic substrates.

In the present work we realized H_2 flux measurements on flat planar $LaWO_{mem}/LaWO_{sub}$ ($LaWO_{mem}$ thickness 30 µm) and $LaWO_{mem}/Crofer_{sub}$ ($LaWO_{mem}$ thickness 60 µm) assemblies fabricated respectively by means of the tape casting and the PS-PVD technology. At 825 °C H_2 flux of ca. 0.4 ml/min·cm^2 was measured for the 60 µm thick $LaWO_{mem}$ PS-PVD deposited on $Crofer_{sub}$ and the same value could be extrapolated for the 30 µm thick $LaWO_{mem}$ tape cast membrane supported on $LaWO_{sub}$. These results compare very well with the available literature data. The value obtained in this work is the highest reported so far for LaWO asymmetric membrane at operation relevant temperatures.

As next aspects of our future work, several mechanical issues need to be addressed as well as membrane performance to be reproduced and the underlying transport effects to be closely explored. It appears very important to increase the mechanical robustness of the tape cast ceramic assemblies, which presently have the overall thickness of up to 500 µm and this leads to mechanical failure during the sealing procedure. Furthermore, as observed the ceramic membrane layer of the PS-PVD fabricated assemblies tend to delaminate therefore preliminary substrate treatment to improve the adhesion before the membrane deposition needs to be envisaged. Additionally, the substrate porosity (tape cast samples) needs to be increased along with optimized Pt activation for improved performance. Finally, to boost the membrane performance assemblies with decreased membrane thickness are aimed. As future prospective scale up of such asymmetric assemblies to industrially relevant component sizes will enable to proof various application concepts.

Acknowledgements

ProtOMem Project under the BMBF grant 03SF0537 is gratefully acknowledged. Furthermore, the authors thank Ralf Laufs for his assistance in operating the PS-PVD facility. Dr. A. Schwedt from the Central Facility for Electron Microscopy (Gemeinschaftslabor für

Elektronenmikroskopie GFE), RWTH Aachen University is acknowledged for performing the EBSD analysis on the PS-PVD samples.

References

[1] A. A. Evers, The hydrogen society. More than just a vision?, ISBN 978-3-937863-31-3, Hydrogeit Verlag, 16727 Oberkraemer, Germany 2010.

[2] W. Deibert, M. E. Ivanova, S. Baumann, O. Guillon, W.A. Meulenberg, Ion-conducting ceramic membrane reactors for high temperature applications, J. Membrane Sci. 543 (2017) 79-97.

[3] Arun C. Bose, Inorganic Membranes for Energy and Environmental Applications, Edt. A. C. Bose, ISBN: 978-0-387-34524-6, Springer Science+Business Media, LLC 2009.

[4] M. Marrony, H. Matsumoto, N. Fukatsu, M. Stoukides, Typical applications of proton ceramic cells: a way to market?, in Proton-conducting ceramics. From fundamentals to applied research, Edt. M. Marrony, by Pan Stanford Publishing Pte. Ltd., ISBN 978-981-4613-84-2 2016.

[5] P. Di Georgio, U. Desideri, Potential of reversible solid oxide cells as electricity storage system, Energies 9 (2016) 662-676.

[6] A. L. Dicks, D. A. J. Rand, Fuel cell systems explained, ISBN: 9781118613528, John Wiley & Sons Ltd.(2018)

[7] Y. Zheng, J. Wang, B. Yu, W. Yhang, J. Chen, J. Oiao, J. Yhang, A review of high temperature co-electrolysis of H_2O and CO_2 to produce sustainable fuels using solid oxide electrolysis cells (SOECs): advanced materials and technology, Chem. Soc. Rev. 46 (2017) 1427-1463.

[8] M. Götz, J. Lefebre, F. Mörs, A. McDaniel Koch, F. Graf, S. Bajohr, R. Reimert, T. Kolb, Renewable power-to-gas: a technological and economic review, Renew. Energy 85 (2016) 1371-1390.

[9] Woodhead publishing series in energy, Nr. 76, Membrane reactors for energy applications and basic chemical production, Edt. A. Basile, L. Di Paola, F. I. Hai, V. Piemonte, by Elsevier Ltd, ISBN 978-1-78242-223-5 2015.

[10] S.H. Morejudo, R. Zanón, S. Escolástico, I. Yuste-Tirados, H. Malerod-Fjeld, P.K.Vestre, W.G. Coors, A. Martínez, T. Norby, J.M. Serra, C. Kjølseth, Direct conversion of methane to aromatics in a catalytic co-ionic membrane reactor, Science 353 (2016) 563-566.

[11] H. Malerod-Fjeld, D. Clark, I. Yuste-Tirados, R. Zanón, D. Catalán-Martínez, D. Beeaff, S.H. Morejudo, P.K. Vestre, T. Norby, R. Haugsrud, J.M. Serra, C. Kjølseth, Thermo-electrochemical production of compressed hydrogen from methane with near-zero energy loss, Nature Energy 2 (12) (2017) 923 - 931.

[12] Franz J. Energetic and economic analysis of CO_2 retention in coal gasification power plants by means of polymer and ceramic membranes (dissertation, German), Ruhr-University Bochum, Germany, Shaker Verlag (2013).

[13] J. Franz, V. Scherer, Impact of ceramic membranes for CO_2 separation on IGCC power plant performance, Energy Procedia 4 (2011) 645 – 652.

[14] E. Forster, dissertation, Thermal stability of ceramic membranes and catalysts for H_2-separation in CO-shift reactors, Energy and Environment Band, vol. 284, ISBN 978-3-95806-084-5, RUB 2015.

[15] S. Escolástico, V. Stournari, J. Malzbender, K. Haas-Santo, R. Dittmeyer, J.M. Serra, Chemical stability in H_2S and creep characterization of the mixed protonic conductor $Nd_{5.5}WO_{11.25-\delta}$, Int. J. Hydrogen Energy 43 (17) (2018) 8342-8354.

[16] C. Mortalò, E. Rebollo, S. Escolástico, S. Deambrosis, K. Haas-Santo, M. Rancan, R. Dittmeyer, L. Armelao, M. Fabrizio, Enhanced sulfur tolerance of $BaCe_{0.65}Zr_{0.20}Y_{0.15}O_{3-\delta}$-$Ce_{0.85}Gd_{0.15}O_{2-\delta}$ composite for hydrogen separation membranes, J. Membrane Sci. 564 (2018) 123-132.

[17] S. Escolástico, C. Solís, T. Scherb, G. Schumacher, J.M. Serra, Hydrogen separation in $La_{5.5}WO_{11.25-\delta}$ membranes, J. Membr. Sci. 444.(2013) 276–284.

[18] H. Matsumoto, T. Shimura, T. Higuchi, H. Tanaka, K. Katahira, T. Otake, T. Kudo, K. Yashiro, A. Kaimai, T. Kawada, J. Mizusaki, Protonic-electronic mixed conduction and hydrogen permeation in $BaCe_{0.9-x}Y_{0.1}Ru_xO_{3-\delta}$, J. Electrochem. Soc. 152(3) (2005) A488-A492.

[19] M. Cai, S. Liu, K. Efimov, J. Caro, A. Feldhoff, H. Wang, Preparation and hydrogen permeation of $BaCe_{0.95}Nd_{0.05}O_{3-\delta}$ membranes, J. Memb. Sci. 343 (2009) 90–96.

[20] U. Balachandran, J. Guan, S.E. Dorris, A.C. Bose,G.J. Stiegel, Proceedings of the 5th ICIM, A-410, Nagoya, Japan (1998)

[21] X. Qi, Y.S. Lin, Electrical conductivity and hydrogen permeation through mixed proton-electron conducting strontium cerate membranes, Solid State Ionics 130 (2000) 149-156.

[22] S. Zhan, X. Zhu, B. Ji, W. Wang, X. Zhang, J. Wang, W. Yang, L. Lin, Preparation and hydrogen permeation of $SrCe_{0.95}Y_{0.05}O_{3-\delta}$ asymmetrical membranes. J. Memb. Sci. 340 (2009) 241–248.

[23] S.J. Song, E.D. Wachsman, J. Rhodes, S.E. Dorris, U. Balachandran, Hydrogen permeability of $SrCe_{1-x}M_xO_{3-\delta}$ (x=0.05, M=Eu,Sm), Solid State Ionics 167 (2004) 99–105.

[24] X. Wei, J. Kniep, Y.S. Lin, Hydrogen permeation through terbium doped strontium cerate membranes enabled by presence of reducing gas in the downstream, J. Memb. Sci. 345 (2009) 201–206.

[25] S.G. Cheng, V.K. Gupta, Y.S. Lin, Synthesis and hydrogen permeation properties of asymmetric proton-conducting ceramic membranes, Solid State Ionics 176 (2005) 2653–2662.

[26] X.W. Qi, Y.S. Lin, Electrical conduction and hydrogen permeation through mixed proton-electron conducting strontium cerate membranes, Solid State Ionics 130 (2000) 149–156.

[27] J. Kniep, Y.S. Lin, Effect of Zirconium doping on hydrogen permeation through Strontium Cerate membranes, Ind. Eng. Chem. Res. 49 (2010) 2768–2774.

[28] J. Liang, L. Mao, L. Li, W. Yuan, Protonic and electronic conductivities and hydrogen permeation of $SrCe_{0.95-x}Zr_xTm_{0.05}O_{3-\delta}$ ($0 \le x \le 0.40$) membrane, Chinese J. Chem. Eng. 18 (2010) 506–510.

[29] W. Xing, P.I. Dahl, L. Valland Roaas, M.-L. Fontaine, Y. Larring, P.P. Henriksen, R. Bredesen, Hydrogen permeability of $SrCe_{0.7}Zr_{0.25}Ln_{0.05}O_{3-\delta}$ membranes (Ln = Tm and Yb), J. Memb. Sci. 473 (2015) 327–332.

[30] T. Oh, H. Yoon, J. Li, E.D. Wachsman, Hydrogen permeation through thin supported $SrZr_{0.2}Ce_{0.8-x}Eu_xO_{3-\delta}$ membranes, J. Memb. Sci. 345 (2009) 1–4.

[31] S. Hamakawa, L. Li, A. Li, E. Iglesia, Synthesis and hydrogen permeation properties of membranes based on dense $SrCe_{0.95}Yb_{0.05}O_{3-\delta}$ thin films, Solid State Ionics 148 (2002) 71–81.

[32] S. Escolástico, M. E. Ivanova, C. Solís, S. Roitsch, W.A. Meulenberg, J.M. Serra, Improvement of transport properties and hydrogen permeation of chemically-stable proton-conducting oxides based on the system $BaZr_{1-x-y}Y_xM_yO_{3-\delta}$, RSC Adv. 2 (2012) 4932-4943.

[33] H. Matsumoto, T. Shimura, T. Higuchi, T. Otake, Y. Sasaki, K. Yashiro, A. Kaimai, T. Kawada, J. Mizusaki, Mixed protonic-electronic conduction properties of $SrZr_{0.9-x}Y_{0.1}Ru_xO_{3-\delta}$, Electrochemistry, 72(12), 861-864

[34] M. E. Ivanova, S. Escolático, M. Balaguer, J. Palisaitis, Y. J. Sohn, W.A. Meulenberg, O. Guillon, J. Mayer, J.M. Serra, Hydrogen separation through tailored dual phase membranes with nominal composition $BaCe_{0.8}Eu_{0.2}O_{3-\delta}$:$Ce_{0.8}Y_{0.2}O_{2-\delta}$ at intermediate temperatures, Sci. Rep. 6 (2016) 34773-34787.

[35] S. Elangovan, B.G. Nair, T.A. Small, Ceramic mixed protonic-electronic conducting membranes for hydrogen separation (2007), US 7,258,820 B2 (1997).

[36] W.A. Rosensteel, S. Ricote, N.P. Sullivan, Hydrogen permeation through dense $BaCe_{0.8}Y_{0.2}O_{3-\delta}$-$Ce_{0.8}Y_{0.2}O_{2-\delta}$ composite-ceramic hydrogen separation membranes, Int. J. Hydrogen Energy 41 (2016) 2598–2606.

[37] E. Rebollo, C. Mortalo, S. Escolástico, S. Boldrini, S. Barison, J.M. Serra, M. Fabrizio, Exceptional hydrogen permeation of all-ceramic composite robust membranes based on $BaCe_{0.65}Zr_{0.20}Y_{0.15}O_{3-\delta}$ and Y- or Gd-doped ceria. Energy Environ. Sci. 8 (2015) 3675–3686.

[38] D. Montaleone, E. Mercadelli, S. Escolástico, A. Gondolini, J.M. Serra, A. Sanson, All-ceramic asymmetric membranes with superior hydrogen permeation, J. Mater. Chem. A 6, (2018) 15718- 15727.

[39] H. Kim, B. Kim, J. Lee, K. Ahn, H.-R. Kim, K.J. Yoon, B.-K. Kim, Y.W. Cho, H.-W. Lee, J.-H. Lee, Microstructural adjustment of Ni–$BaCe_{0.9}Y_{0.1}O_{3-\delta}$ cermet membrane for improved hydrogen permeation. Ceram. Int. 40 (2014) 4117–4126.

[40] U. Balachandran, T.H. Lee, C.Y. Park, J.E. Emerson, J.J. Picciolo, S.E. Dorris, Dense cermet membranes for hydrogen separation, Sep. Purif. Technol. 121 (2014) 54–59.

[41] T. Shimura, S. Fujimoto, H. Iwahara, Proton conduction in non-perovskite-type oxides at elevated temperatures, Solid State Ionics 143 (2001) 117-123.

[42] R. Haugsrud, Defects and transport properties in Ln_6WO_{12} (Ln=La, Nd, Gd, Er), Solid State Ionics 178 (2007) 555-560.

[43] R. Haugsrud, C. Kjolseth, Effects of protons and acceptor substitution on the electrical conductivity of La_6WO_{12}, J. Phys. Chem. Solids 69 (2008) 1758-1765.

[44] A. Magrasó, C. Frontera, D. Marrero-López, P. Núñez, New crystal structure and characterization of lanthanum tungstate "La_6WO_{12}" prepared by freeze-drying synthesis, Dalton Trans. (2009) 10273-10283.

[45] A. Magrasó, J. Polfus, C. Frontera, J. Canales-Vázquez, L.-E. Kalland, C. Hervoches, S. Erdal, R. Hancke, M. Saiful Islam, T. Norby, R. Haugsrud, Complete structural model for lanthanum tungstate: a chemically stable high temperature proton conductor by means of instrinsic defects, J. Mater. Chem. 22 (2012) 1762-1764.

[46] J. Seeger, M. E. Ivanova, W. A. Meulenberg, D. Sebold, D. Stöver, T. Scherb, G. Schumacher, S. Escolástico, C. Solís, J. M. Serra, Synthesis and characterization of nonsubstituted and substituted proton conducting $La_{6-x}WO_{12-\delta}$, Inorg. Chem. 52 (2013) 10375-10386.

[47] T. Scherb, S. A.J. Kimber, C. Stephan, P. F. Henry, G. Schumacher, S. Escolástico, J.M. Serra, J. Seeger, J. Just, A. H. Hill, J. Banhart, Nanoscale order in the frustrated mixed conductor $La_{5.6}WO_{12-\delta}$, J. Appl. Cryst. 49 (2016) 997-1008.

[48] D. van Holt, E. Forster, M. E. Ivanova, W. A. Meulenberg, M. Müller, S. Baumann, R. Vaßen, Ceramic materials for H_2 transport membranes applicable for gas separation under coal-gasification related conditions, J. Eur. Ceram. Soc. 34 (2014) 2381-2389.

[49] E. Forster, D. Van Holt, M. E. Ivanova, S. Baumann, W. A. Meulenberg, M. Müller, Stability of ceramic materials for H_2 transport membranes in gasification environment under the influence of gas contaminants, J. Eur. Ceram. Soc. 36 (2016) 3457-3464.

[50] D. Medvedev, J. Lyagaeva, S. Plaksin, A. Demin, P. Tsiakaras, Sulfur and carbon tolerance of $BaCeO_3$-$BaZrO_3$ proton-conducting materials, J. Power Sources 273 (2015) 716-723.

[51] L. Yang, S. Wang, K. Blinn, M. Liu, Z. Liu, Z. Cheng, M. Liu, Enhanced sulfur and coking tolerance of a mixed ion conductor for SOFCs: $BaZr_{0.1}Ce_{0.7}Y_{0.2-x}Yb_xO_{3-\delta}$, Science 326 (5949) (2009) 126–129.

[52] C. Duan, R.J. Kee, H. Zhu, C. Karakaya, Y. Chen, S. Ricote, A. Jarry, E.J. Crumlin, D. Hook, R. Braun, N. P. Sullivan, R. O'Hayre, Highly durable, coking and sulfur tolerant, fuel-flexible protonic ceramic fuel cells, Nature 557 (2018) 217–222.

[53] C. Mortallo, E. Rebollo, S. Escolástico, S. Deambrosis, K. Haas-Santo, M. Rancan, R. Dittmeyer, L. Armelao, M. Fabrizio, Enhanced sulfur tolerance of $BaCe_{0.65}Zr_{0.20}Y_{0.15}O_{3-\delta}$-$Ce_{0.85}Gd_{0.15}O_{2-\delta}$ composite for hydrogen separation membranes, J. Membr. Sci. 564 (2018) 123–132.

[54] K.-D. Kreuer, Proton-Conducting Oxides, Annual Review of Materials Research 33 (2003) 333–359.

[55] M. E. Ivanova, J. Seeger, J.M. Serra, C. Solis, W.A. Meulenberg, W. Fischer, S. Roitsch, H.P. Buchkremer, Chem. Mater. Res. 2 (2012) 56−81.

[56] A. Fantin, T. Scherb, J. Seeger, G. Schumacher, U. Gerhards, M. E. Ivanova, W. A. Meulenberg, R. Dittmeyer, J. Banhart, Crystal structure of Re-substituted lanthanum tungstate $La_{5.4}W_{1-y}Re_yO_{12-\delta}$ ($0 \le y \le 0.2$) studied by neutron diffraction, J. Appl. Cryst. 49 (2016) 1544-1560.

[57] A. Fantin, T. Scherb, J. Seeger, G. Schumacher, U. Gerhards, M. E. Ivanova, W.A. Meulenberg, R. Dittmeyer, J. Banhart, Relation between composition and vacant oxygen sites in the mixed ionic-electronic conductors $La_{5.4}W_{1-y}M_yO_{12-\delta}$ (M=Mo,Re; $0 \le y \le 0.2$) and their mother compound $La_{6-x}WO_{12-\delta}$ ($0.4 \le x \le 0.8$), Solid State Ionics 306 (2017) 104-111.

[58] J.M. Serra, S. Escolástico, M.E. Ivanova, W.A. Meulenberg, H.-P. Buchkremer, D. Stöver, US2013-0216938-A1 (2013).

[59] S. Escolástico, J. Seeger, S. Roitsch, M. E. Ivanova, W. A. Meulenberg, J. M. Serra, Enhanced H_2 separation through mixed proton-electron conducting membranes based on $La_{5.5}W_{0.8}M_{0.2}O_{11.25-\delta}$, ChemSusChem 6 (2013) 1523-1532.

[60] V. Gil, J. Gurauskis, M. A. Einarsrud, Asymmetric supported dense lanthanum tungstate membranes, J. Eur. Ceram. Soc. 34 (2014) 3783–3790.

[61] V. Gil, J. Gurauskis, C. Kjølseth, K. Wiik, M.A. Einarsrud, Hydrogen permeation in asymmetric $La_{28-x}W_{4+x}O_{54+3x/2}$ membranes, Int. J. Hydrogen Energy 38 (2013) 3087–3091.

[62] G. Howatt, R.G. Breckenridge, J.M. Brownlow, Fabrication of thin ceramic sheets for capacitors, J. Am. Cer. Soc., 30 (1947) 237-242.

[63] L. Palmqvist, K. Lindqvist, C. Shaw, Porous multilayer PZT materials made by aqueous tape casting, Key Eng. Mat. 333 (2007) 215-218.

[64] N. H. Menzler, J. Malzbender, P. Schoderböck, R. Kauert, H. P. Buchkremer, Sequential tape casting of anode-supported Solid Oxide Fuel Cells, Fuel Cells 14 (2013) 96-106.

[65] F. Schulze-Küppers, S.Baumann, F. Tietz, H.J.M. Bouwmeester, W.A. Meulenberg, Towards the fabrication of $La_{0.98-x}Sr_xCo_{0.2}Fe_{0.8}O_{3-\delta}$ perovskite-type oxygen transport membranes, J. Eur. Cer. Soc. 34 (2014) 3741-3748.

[66] M. Weirich, J. Gurauskis, V. Gil, K. Wiik, M.-A. Einarsrud, Preparation of lanthanum tungstate membranes by tape casting technique, Int. J. Hydrogen Energy, 37 (2012) 8056-8061.

[67] W. Deibert, M. E. Ivanova, W. A. Meulenberg, R. Vaßen, O. Guillon, Preparation and sintering behaviour of $La_{5.4}WO_{12-\delta}$ asymmetric membranes with optimized mictrostructure for H_2 separation, J. Membrane Sci. 492 (2015) 439-451.

[68] W. Deibert, F. Schulze-Küppers, E. Forster, M. E. Ivanova, M. Müller, W. A. Meulenberg, Stability and sintering of MgO as a substrate materials for Lanthanum tungstate membranes, J. Eur. Ceram. Soc. 37 (2017) 671-677.

[69] S. Escolástico, V.B. Vert, J.M. Serra, Preparation and characterizationof nanocrystalline mixed proton-electronic conducting materials based on the system La_6WO_{12}, Chem. Mater. 21 (2009) 3079-3089.

[70] V. Gil, R. A. Strøm, L. J. Groven and M.-A. Einarsrud, $La_{28-x}W_{4+x}O_{54+3x/2}$ powder prepared by spray pyrolysis, J. Am. Ceram. Soc. 95 (2012) 3403-3407.

[71] M. E. Ivanova, W.A. Meulenberg, J. Palisaitis, D. Sebold,C. Solís, M. Ziegner, J.M. Serra, J. Mayer, M. Hänsel, O. Guillon, Functional properties of $La_{0.99}X_{0.01}Nb_{0.99}Al_{0.01}O_{4-\delta}$ and $La_{0.99}X_{0.01}Nb_{0.99}Ti_{0.01}O_{4-\delta}$ proton conductors where X is an alkaline earth cation, J. Eur. Cer. Soc. 35 (2015) 1239–1253.

[72] R. Dittmeyer, T. Boeltken, P. Piermartini, M. Selinsek, M. Loewert, F. Dallmann, H. Kreuder, M. Cholewa, A. Wunsch, M. Belimov, S. Farsi, P. Pfeifer, Micro and micro membrane reactors for advanced application in chemical energy conversion, Curr. Opin. Chem. Eng. 17 (2017) 108-125.

[73] G. Mauer, R. Vaßen, D. Stöver, Thin and dense ceramic coatings by plasma spraying at very low pressure, J. Therm. Spray Technol. 19 (2010) 495-501.

[74] E. Bakan, R. Vaßen, Ceramic top coats of plsama-sprayed thermal barrier coatings: materials, processes, and properties, J. Therm. Spray Tech. 26 (2017) 992-1010.

[75] M.O. Jarligo, G. Mauer, M. Bram, S. Baumann, R. Vaßen, Plasma Spray Physical Vapor Deposition of $La_{1-x}Sr_xCo_yFe_{1-y}O_{3-\delta}$ thin-film oxygen transport membrane on porous metallic supports, J. Therm. Spray Technol. 23 (2014) 213-219.

[76] D. Marcano, G. Mauer, Y.J. Sohn, R. Vaßen, J. Garcia-Fayos, J.M. Serra, Controlling the stress state of $La_{1-x}Sr_xCo_yFe_{1-y}O_{3-\delta}$ oxygen transport membranes on porous metallic supports deposited by plasma spray-physical vapor process, J. Membrane Sci. 503 (2016) 1-7.

[77] D. Marcano, G. Mauer, R. Vaßen, A. Weber, Manufacturing of high performance solid oxide fuel cells (SOFCs) with atmospheric plasma spraying (APS) and plasma spray-physical vapor deposition (PS-PVD), Surf. Coatings Technol. 318 (2017) 170–177.

[78] D. Marcano, G. Mauer, Y. J. Sohn, A. Schwedt, M.Bram, M. E. Ivanova, R. Vaßen, Plasma Spray-Physical Vapor Deposition of single phase Lanthanum tungstate for hydrogen gas separation membranes, t.b. submitted (2018).

[79] S. Brunauer, P. Emmett, E. Teller, Adsorption of Gases in Multimolecular Layers, J. Am. Chem. Soc. 60 (1938) 309-319.

[80] P. Ried, C. Lorenz, A. Brönstrup, T. Graule, N.H.Menzler, W. Sitte, P. Holtappels, Processing of YSZ screen printing pastes and the characterization of the electrolyte layers for anode supported SOFC, J. Eur. Cer. Soc. 28 (2008) 1801–1808.

[81] R. Mücke, Sintering of ZrO_2- electrolytes in multilayered assemblies of SOFC, PhD Thesis, Ruhr-University, Bochum (2007).

[82] M. Amsif, A. Magrasó, D. Marrero-Lopey, J. C. Ruiz-Morales, J. Canales-Vazquez, P. Nunez, Mo-substituted Lanthanum tungstate: a competitive mixed electron-proton conductor for gas separation membrane applications, Chem. Mater. 24 (2012) 3868-3877.

[83] A. U. Daniels, R. C. Lowrie, R. L. Gibby, I. B. Cutler, Observations on normal grain growth of Magnesia and Calcia, J. Amer. Ceram. Soc. 45 (1962) 282-285.

Supplementary Information

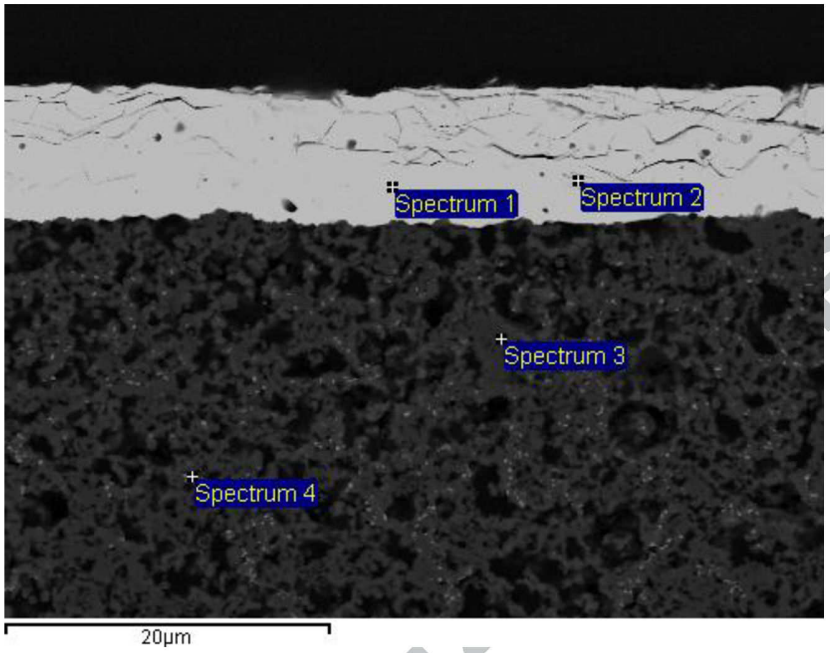

Figure S1 a. SEM image of a polished cross section of Mo-$LaWO_{mem}/MgO_{sub}$ assembly sintered at 1450 °C for 6h.

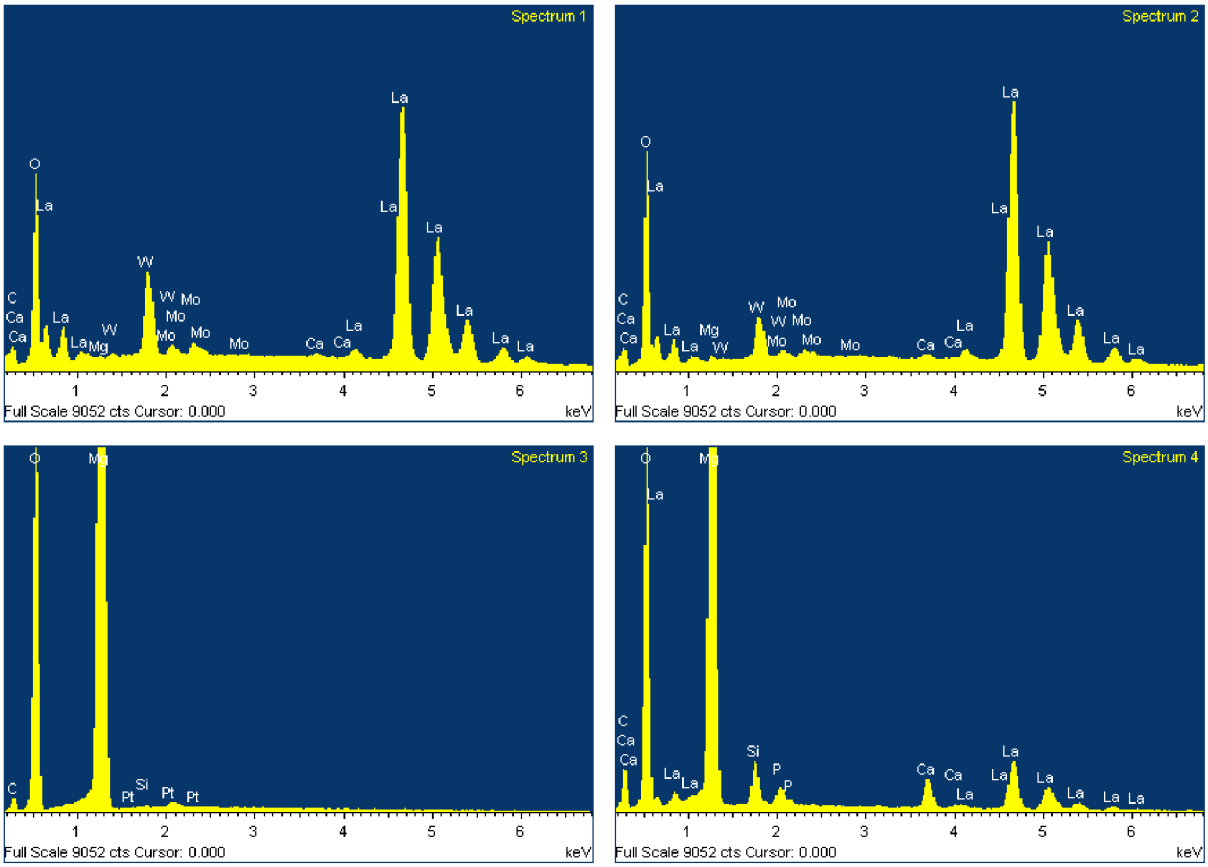

Figure S1 b. EDX spectra for the Mo-LaWO$_{mem}$ (Spectra 1 and 2) and for the MgO$_{sub}$ (Spectra 3 and 4). Data show clearly the absence of Mo in the substrate.